



Article

Observation and Data Reduction of the Brown Dwarf 2MASSW J0746425 + 200032 by Five-Hundred-Meter Aperture Spherical Radio Telescope

Tianhao Su ¹, Liyun Zhang ^{1,*} , Xuyang Gao ², Qingfeng Pi ³, Prabhakar Misra ⁴  and Xianming L. Han ⁵

¹ Guizhou Provincial Key Laboratory of Public Big Data, College of Physics, Guizhou University, Guiyang 550025, China; su.tian.hao@outlook.com

² National Astronomical Observatories, Chinese Academy of Sciences, Beijing 100101, China; xygao@nao.cas.cn

³ College of Medicine, Guizhou University of Traditional Chinese Medicine, Guiyang 550025, China; piqingfeng@126.com

⁴ Department of Physics & Astronomy, Howard University, Washington, DC 20059, USA; pmisra@howard.edu

⁵ Department of Physics and Astronomy and SARA, Butler University, Indianapolis, IN 46208, USA; xhan@butler.edu

* Correspondence: liy_zhang@hotmail.com

Abstract: The unprecedented sensitivity provided by the Five-hundred-meter Aperture Spherical radio Telescope (FAST) could shed light on studies of the magnetic field and plasma properties of brown dwarfs by catching polarized radio flares. With the FAST L-band 19-beam receiver, we observe a nearby dwarf stellar system 2MASSW J0746425 + 200032 which has been reported to show 4.86 GHz and 8.46 GHz radio flare emission. The L-band radio signals from the target are searched in both total intensity and circular polarization during the entire 147 min tracking observation. No radio flare down to a sensitivity of ~ 13 mJy and ~ 2 mJy (5σ) in Stokes I and V can be identified. The non-detection may lie in the intrinsic physical condition of the stellar system, e.g., the magnetic field strength and the electron density distribution and/or the sampling rate, which should be higher to reveal the sub-second structures but are smeared out with a lower rate in our observations.



Citation: Su, T.; Zhang, L.; Gao, X.; Pi, Q.; Misra, P.; Han, X.L. Observation and Data Reduction of the Brown Dwarf 2MASSW J0746425 + 200032 by Five-Hundred-Meter Aperture Spherical Radio Telescope. *Universe* **2023**, *9*, 360. <https://doi.org/10.3390/universe9080360>

Academic Editor: Ana Inés Gómez de Castro

Received: 1 July 2023

Revised: 31 July 2023

Accepted: 31 July 2023

Published: 3 August 2023



Copyright: © 2023 by the authors. Licensee MDPI, Basel, Switzerland. This article is an open access article distributed under the terms and conditions of the Creative Commons Attribution (CC BY) license (<https://creativecommons.org/licenses/by/4.0/>).

Keywords: browndwarf; data analysis; individual; 2MASSW J0746425 + 200032

1. Introduction

Radio emission from stars and stellar systems has drawn a great attention and become a hotspot in today's radio astronomy. A pioneering and profound work was performed by Wendker [1], providing a catalog that contains 3699 single stars and binary systems, together with stellar parameters and radio intensities at various frequencies. With the promotion of sensitivity brought by the large single-dish radio telescopes and high angular resolution of the interferometric arrays, the research of radio stars has achieved rapid progress in recent years. Güdel [2] collected the radio intensity of stars with different types and made the stellar radio Hertzsprung–Russell diagram. They found that radio radiation can come from early- to late-type stars and also from different stellar systems, e.g., RS CVn binaries [3], W Uma and Algol eclipsing binaries [4,5], ultra-cool dwarfs [6], low-mass stars [7], and main sequence stars [8]. Radio observations toward stars and stellar systems can reveal many physical phenomena and processes, such as stellar magnetic activity, particle acceleration, mass transfer between two components of binaries, and interactions between stars, planets, and stellar winds [3,9,10]. At present, tens of thousands of stars are found to show radio radiation [1,11].

Ultra-cool dwarfs (UCDs) refer to extremely low-temperature, extremely low-mass stars, and brown dwarfs with a spectral type of M7 or later [12,13]. They are so faint that only nearby UCDs can be detected to date [14–16]. Williams et al. [17] found that some UCDs are radio-overluminous relative to the Güdel–Benz relation [18,19]. The latest

research indicates that more than 3% of UCDs could show radio flares (e.g., [20]). The radio radiation of UCDs is suggested to consist of gyrosynchrotron emission from a population of mildly relativistic electrons [21] and the electron–cyclotron maser [22]. The former is the main mechanism for the quiescent radiation, while the latter is for the flare emission.

2MASSW J0746425 + 200032 is a close binary system (e.g., [23]) at a distance of about 12.2 pc [24]. Bouy et al. [25] derived a spectral type of $L0 \pm 0.5$ and $L1.5 \pm 0.5$ for its two components 2M0746A and 2M0746B, respectively. Reid et al. [26] found that the system shows H α emission, which was explained by the chromospheric activity. Berger et al. [27] presented the observations of 2MASSW J0746425 + 200032 in radio, X-ray, UV, and H α . They detected a series of bright radio emissions (10–15 mJy) with total intensity I and nearly 100% circular polarization V with short-duration (~ 1.2 min) pulses at 4.86 GHz and a period of 124.32 ± 0.11 minutes by using the Very Large Array (VLA). The H α emission was also found to show a periodic change with the same time interval. However, the simultaneous observation at 8.46 GHz showed no corresponding emission to that of 4.86 GHz, but successfully traced another single pulse. Harding et al. [28] detected a period of 3.32 ± 0.15 h toward 2MASSW J0746425 + 200032 by using the 1.83-m optical telescope of the Vatican observatory, pointing out that the observed period of 124.32 ± 0.11 min of the radio pulses at 4.86 GHz is associated with the secondary star in the binary system. Zhang et al. [29] used the Very Long Baseline Array (VLBA) to track the radio emission of 2MASSW J0746425 + 200032 of about 22.5 h in seven epochs during the years of 2010–2017. They found that both UCDs in the system show radio emission. All above observations were made above 4 GHz. A few UCDs were observed by using the Giant Metrewave Radio Telescope (GMRT) at 610 MHz and 1300 MHz [30], including 2MASSW J0746425 + 200032. It was the first time to observe this binary system at this low radio frequency. A quiescent radio emission component over 300 mJy was found at both frequencies. No radio flare was detected.

The Five-hundred-meter Aperture Spherical radio Telescope (FAST) is the largest single-dish radio telescope in the world, which provides unprecedented sensitivity [31]. The $\sim 3'$ angular resolution of FAST in comparison to that of the radio interferometers is that it may be difficult to extract the signal from the stars/stellar systems in total intensity, due to the higher confusion limit [32,33]. Fortunately, the stellar radio flare induced by ECM presents high degree of circular polarization, e.g., 100% [34–38], toward which a much lower confusion limit can be reached (e.g., [20,39]). Treumann [40] emphasized in their review that the ECM is a powerful diagnostic tool to investigate the magnetic field strength and the electron density in radio sources. Therefore, we targeted 2MASSW J0746425 + 200032 with a limited FAST observation time, aiming to detect its radio flare emission at the L-band. The work is structured as below. A brief introduction of our FAST observation and data reduction are presented in Section 2. The observational results are shown in Section 3, and we summarize at last in Section 4.

2. Observation and Data Reduction

2.1. Observation

FAST has an effective collecting area with a 300 m diameter, and is equipped with a 19-beam receiver working at the L-band, covering the frequency range of 1.0–1.5 GHz. The angular resolution is about $3'$ at 1.47 GHz and about $3.8'$ at 1.04 GHz [41]. The total 500 MHz bandwidth can be split into 64k or 1024k channels by the spectroscopy backend. The FAST L-band observation of 2MASSW J0746425 + 200032 was made on 30 April 2021. We used the 64k channel output from the spectroscopy backend. In order not to miss the 1.2 min duration flare [27] when slewing the telescope, the traditional “beam-switching” or “on–off” modes were not applied. Instead, the target source was always tracked by the FAST central beam M01, while data recording is simultaneously activated for the other 18 offset beams to recognize radio frequency interference (RFI). Considering the ~ 124 min period of the radio pulsation detected at 4.86 GHz for 2MASSW J0746425 + 200032 [27], the tracking lasted for 147 min without any breaks, aiming to catch at least one flare if

the stellar system is active at the L-band. The sampling rate of the backend was set to 1 s, and a reference signal with the known intensity of about 1.1 K was injected every other second to calibrate the drift of the system gain. A nearby secondary flux density calibrator was planned, but the observations failed due to improper settings. Therefore, to convert the received radio power to the unit of main-beam brightness temperature, we adopted the frequency-dependent FAST system gain values and the conversion factors between antenna temperature and brightness temperature reported in Gao et al. [41].

2.2. Data Reduction

The output from the FAST spectroscopy backend for the stellar emission can be reduced similarly to that for the radio continuum. The detailed data processing procedure can be found in Sun et al. [42] and Gao et al. [41]. The four correlations of XX, YY, XY, and YX are used to derive the full Stokes parameters, i.e., the sum and the difference between XX and YY yield Stokes I and Q , while 2XY and 2YX give Stokes U and V (e.g., [43,44]). The first step for all the raw data is RFI flagging. Several methods have been reported, e.g., clipping the 3-sigma level of the the median of the absolute deviation from the median (MAD) as performed in Sun et al. [42]. Gao et al. [41] pointed out that the asymmetrically reweighted penalized least squares (ArPLs) algorithm [45] has a good performance on baseline fitting. We use the ArPLs to fit the baseline of the bandpass at each sampling time and make comparisons between the fitted baseline and the observed bandpass. The bandpass at which frequencies show jumps/spikes exceeding 2σ levels of the baseline are flagged. The second step is to calibrate the four observed Stokes parameters to their true quantities by removing instrumental effects. Based on the polarization properties of the injected reference signal, Sun et al. [42] calibrated the differential gain between Stokes I and Q , and the differential phase between Stokes U and V , characterized by two parameters f and χ , respectively. The 100% linear-polarized reference signal was injected to the two orthogonal linear feeds at an angle of 45° ; therefore, $U_{ref} = I_{ref}$ and $Q_{ref} = V_{ref} = 0$ are expected. It is then straightforward to obtain the values of the two parameters f and χ via:

$$f = \frac{Q_{ref}}{I_{ref}}, \tag{1}$$

$$\chi = \frac{1}{2} \arctan \frac{V_{ref}}{U_{ref}}, \tag{2}$$

where ref stands for the reference signal. By applying f and χ to the observational data, we obtain the true Stokes parameters of 2MASSW J0746425 + 200032, following:

$$I_{true} = \frac{I_{obs} - fQ_{obs}}{1 - f^2}, \tag{3}$$

$$Q_{true} = \frac{Q_{obs} - fI_{obs}}{1 - f^2}, \tag{4}$$

$$U_{true} = V_{obs} \sin(2\chi) + U_{obs} \cos(2\chi), \tag{5}$$

$$V_{true} = -U_{obs} \sin(2\chi) + V_{obs} \cos(2\chi) \tag{6}$$

where the subscripts obs and $true$ denote the observed and the calibrated Stokes parameters of the observation. Zhang et al. [46] recently revealed the fine radio flare emission in sub-second time scale from AD Leo with the FAST L-band observations. The same polarization calibration procedure was adopted (see their Appendix A). In this work, we also focus on the total intensity I and the circular polarization V . The calibration procedure is verified through the entire FAST L-band by using the publicly available FAST On-The-Fly observations of 3C 286 (April 2021), whose circular polarization fraction V is 0. We here take the data centered at 1.4 GHz with a 20 MHz bandwidth for a simple demonstration. We derive the Stokes I_{cor} , V_{obs} , and V_{cor} , where the subscripts of cor and obs indicate the

parameters are either calibrated or as observed. The observed V_{obs} of 3C 286 is about -20.6 K T_b and reduced to $V_{cor} \sim 0.8 \text{ K T}_b$ after calibration, equaling a $|V/I|$ ratio change from 8% to 0.3%. We show the V_{obs} and V_{cor} patterns slightly smoothed to the resolution of $4'$ in Figure 1 for indication of changes. The same test is performed for 3C 138. A compatible result ($V_{cor}/I_{cor} \sim 0.4\%$) is achieved. The V/I value after correction is higher than those after high-order corrections (e.g., [47]). However, Myserlis et al. [48] indicated that 3C 286 may show non-zero circular polarization (see their Table 9), but still close to 0. In any case, our result is fine for V detections that show a significant circular polarization fraction.

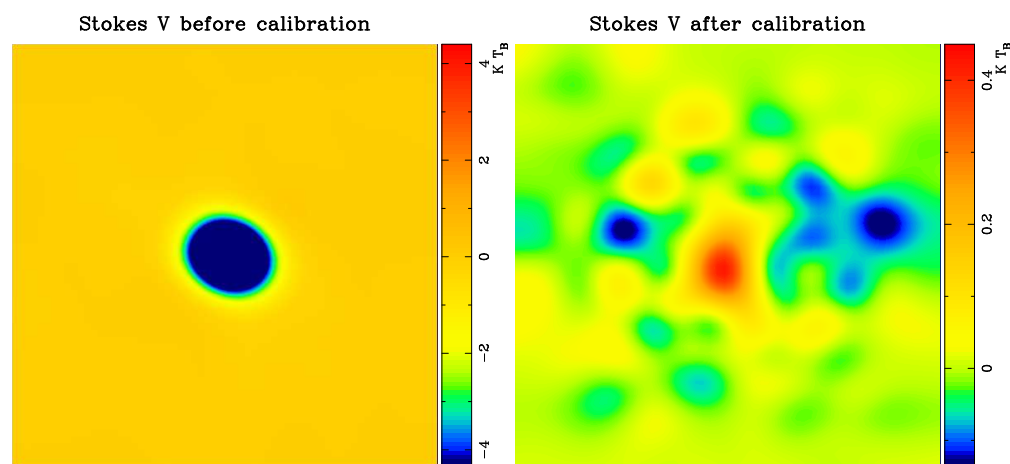


Figure 1. The patterns of the Stokes V of 3C 286 at 1.4 GHz before (left panel) and after (right panel) calibration. The data are convolved to a resolution of $4'$.

The central beam M01 was always on 2MASSW J0746425 + 200032. No off-source data is available for base level estimate. Thus, the received power consists of the possible flare, the quiescent radio emission from the stellar system, and the FAST system temperature, which includes the unrelated galactic background. We examine the power received by the offset FAST beams, e.g., beam M02–beam M19, aiming to estimate the base level of the central beam M01. However, such attempts failed due to the different system gain curves varying with the time between different beams. Therefore, we cannot study the quiescent emission of the stellar system (e.g., [30]) with our observation. However, the flare signal, which shares similarities in RFI in the time and frequency domains, can be recorded in the first step of RFI flagging. After all these processes, we obtained two sets of data: singled-out RFI images and the residual images after RFI elimination both for Stokes I and V . They are used for the search of radio flare of 2MASSW J0746425 + 200032.

3. Results

We show the dynamic spectrum of the singled-out RFI in total intensity I and circular polarization V in the upper panels of Figure 2. We believe that is highly possible to flag the narrow-band and short-time scale flare as RFI. We only present the data in the time length of 7500 s, instead of the entire ~ 8800 s, because of the rapidly increased system temperature and radio frequency interference at the end of the observation. From the image, about half of the frequency channels had severe interference, especially in the range of 1150 MHz to 1270 MHz and those above 1450 MHz. This is consistent with the previous investigations of Wang et al. [49] and Zhang et al. [50]. Due to the limited resolution of the display, the details in the dynamic spectrum both in the dimensions of time and frequency are difficult to be shown clearly. We selected one area in each spectrum of I and V and showed the zoomed-in figures in the lower panels of Figure 2, which showcase the “RFI” near 1420 MHz in I , the HI emission without Doppler correction, and the real RFI in frequency channels around 1090 MHz in V .

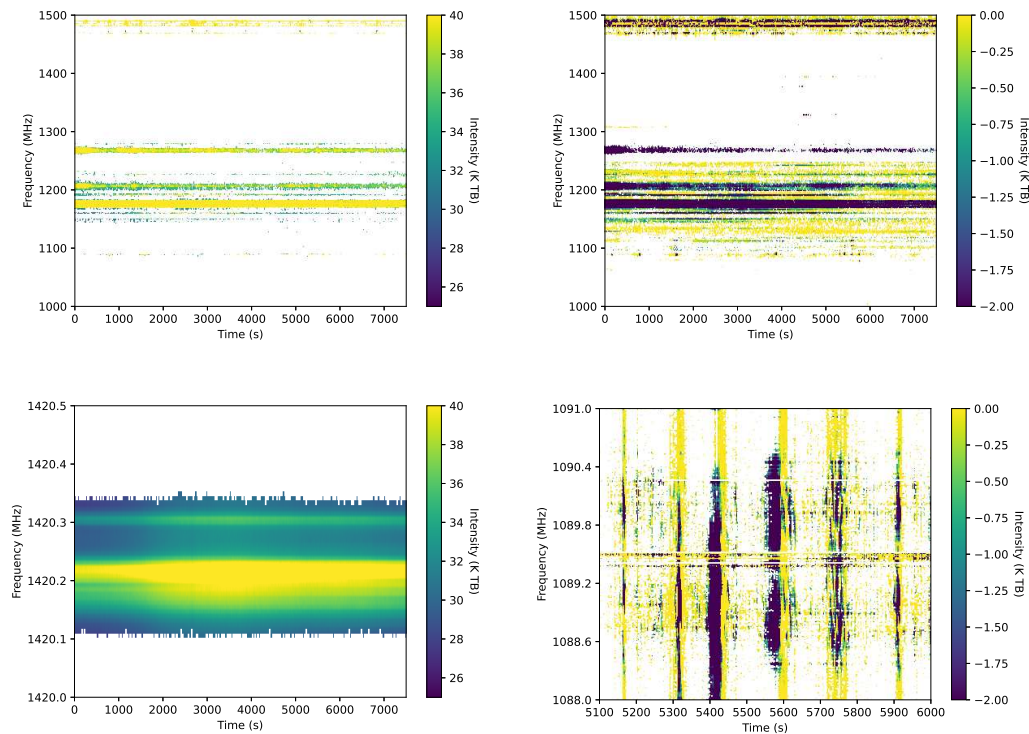


Figure 2. Singled-out RFI in total intensity I (upper left panel) and circular polarization V (upper right panel) of the central beam M01 (on-source). Zoomed-in view around 1420 MHz in Stokes I (lower left panel) and around 1090 MHz in Stokes V (lower right panel).

The flare emission of 2MASSW J0746425 + 200032 at 4.86 GHz shows a period of 124.32 min [27]. If this periodical emission stays at the L-band, only one or two flare emission could be caught in our observation. Therefore, it is not possible to adopt the Fourier transform for an effective search for this apparent periodical signals as for pulsars. Based on another characteristic of the flare, the 1.2 min duration [27], we separated the RFI images in I and V into many $500\text{-s} \times 40\text{ MHz}$ windows, and paid more attention to the RFI signals appearing both in I and V . These sub-sections of the dynamic spectra are carefully examined by eye, aiming to find the evidence of flare emission. However, this is difficult because the data is not only affected by the true and strong RFI, it is also non-trivial to distinguish between the true narrow-band short-time scale RFI and the possible flare signal. 2MASSW J0746425 + 200032 is so close to us that the dispersion measure of 0.13 pc cm^{-3} estimated by Yao et al. [51] cannot make a noticeable effect in our data, even through the entire 1.0–1.5 GHz FAST band ($\tau \sim 0.3\text{ ms}$) regarding the 1 s sampling rate with the spectroscopy backend. Referring to the results of Zhang et al. [46], if further observations can be made, a higher temporal resolution is required for a better recognition of flare signals.

Nevertheless, a few blob structures are noticed, especially in the Stokes V . We aim to further identify these features by the percentage of circular polarization. It is known that the ECM is highly circular polarized, e.g., [20]. The recent FAST observations toward AD Leo show that the radio flare emission generally has a circular polarization fraction of $V/I > 20\%$. We therefore calculate the ratio of V/I for the RFI images. This filtered out the the pixels with $|V/I| < 20\%$ and $|V/I| > 1$, which might be caused by the system jumps and have non-physical sense. The pixels which qualify this criterion are very limited. However, a few blobs are still present in the frequency range of 1080–1100 MHz (see Figure 3). They show a duration of about 30 s, similar to the observed flare at 4.86 GHz, which has a half-power width of about 30 s (see Figure 2 in [27]). However, these features appear several times with similar widths both in time and frequency, which makes us to speculate that they may not be astrophysical. High time resolution observations, e.g., $\sim 49\text{ }\mu\text{s}$ sampling

with the FAST pulsar backend, are needed to discriminate them from RFI by examining if sub-second structures specific to the stellar flare, e.g. frequency drifts are presented.

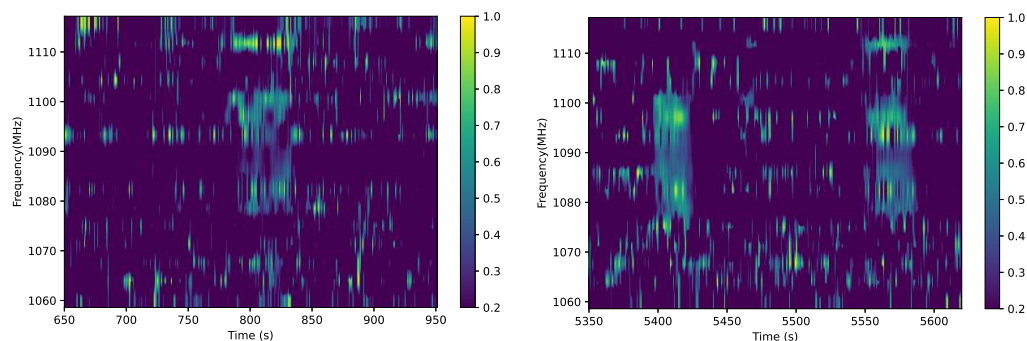


Figure 3. The remaining blob structures selected with $V/I > 20\%$.

Besides searching in the singled-out RFI images, we performed a five-level wavelet analysis of the RFI-subtracted data using Daubechies 4 wavelets, in case the flare is not recognized as RFI. The method is both applied to the Stokes I and V . However, the results are too noisy in V . We therefore only focus on the result of I , and show the results in Figure 4. The left panels in Figure 4 show the dynamic spectrum of I in M01 without RFI and its wavelet analysis results, while the right panels show the same results, but for the FAST offset beam M02. Through comparing the structural features in both beams, no pronounced features that can be clearly identified as flare signals are noticed. The spikes shown in level 1 and level 2 of M01 reflect a short-time depression in I at about 2650 s throughout the 1.0–1.5 GHz band.

The r.m.s value of the RFI-subtracted I data is measured to be about 32 mK T_B , corresponding to ~ 2.6 mJy. For the circular polarization V , the r.m.s is about 5 mK T_B , which is equal to ~ 0.4 mJy. It is reported that the theoretical FAST confusion limit of I is about 1.6 mJy [39], about the same level as found in our data. Our higher value may come from the remaining weak RFI. As a test, we add random signals which are approximately 30–70 s with a bandwidth of about 100 MHz, and an intensity of three to five times the r.m.s value. These signals can be successfully identified through wavelet analysis, especially for the signals with a 5σ level. This demonstrates that the flare if exist in the RFI-subtracted data is not strong enough to be picked out.

The non-detection of the radio flare emission of 2MASSW J0746425 + 200032 at L-band is not odd. The GMRT observations made at 1.3 GHz also failed to detect its radio flare emission [30]. The ECM, which is regarded as responsible for the stellar radio flare, emits mainly at the frequency of $\nu_c \sim 2.8 \times B$ (e.g., [20]). Taking the central observing frequency of 1.25 GHz of the FAST L-band, the object should have a magnetic component with a field strength of about 450 G, which might not be the case for the current status of 2MASSW J0746425 + 200032.

There are significant limitations to the escape of radiation caused by ECM emission from the stellar corona. The emission generated at the fundamental and the second harmonic of the electron cyclotron frequency should be absorbed in the stellar corona at the second and the third cyclotron harmonic layers. Observations made by Berger et al. [52] in the X-ray band indicate that the coronal temperature of brown dwarfs is very high, which contributes to the cyclotron absorption of ECM radiation. This causes the radiation to escape from the star only through two quite narrow “parallel” and “perpendicular” windows Melrose and Dulk [53], Robinson [54]. If there is no proper radiation pattern in the emission source, no ECM radiation will be observed.

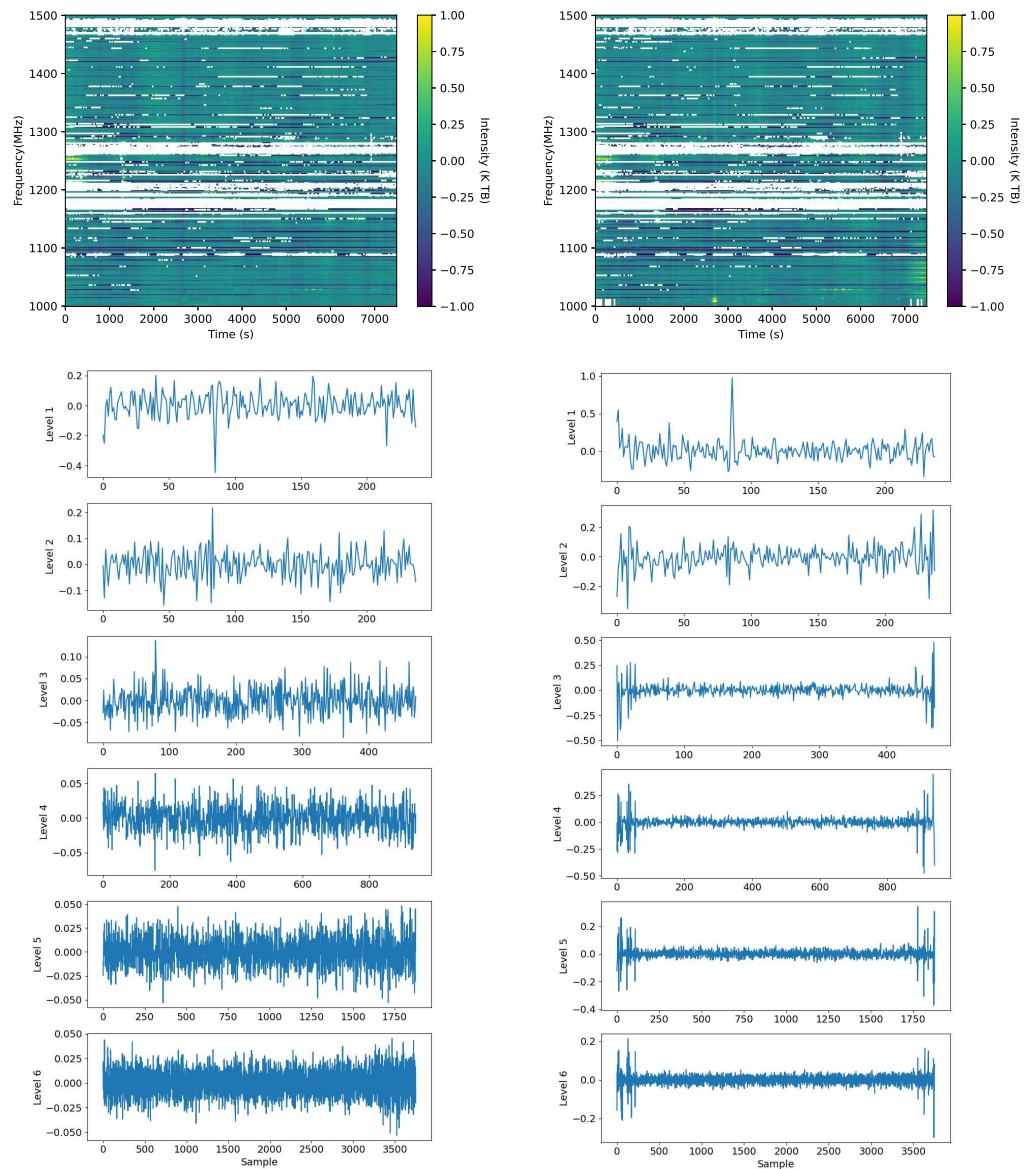


Figure 4. The dynamic spectrum and the wavelet analysis results of M01 without RFI (left panels), and the same results but for M02 (right panels).

In addition, Osten et al. [55] and Berger et al. [27] introduced the quiescent continuous radio emission from a super-cold dwarf star. They believed that this radio emission was caused by cyclotron synchrotron radiation. However, due to our observation mode, we do not include an “off” position. In the process of recognition of RFI through baseline fitting, the quiescent radio radiation that may be generated by the target source is also removed. Therefore, the spectral index of 2MASSW J0746425 + 200032 and its quiescent radiation cannot be obtained from our observation.

4. Summary

Radio polarization observations toward ultra-cool dwarfs provide valuable insight into their physical properties of magnetic field. With the FAST L-band 19-beam receiver, we observe the binary system of 2MASSW J0746425 + 200032, which was reported to show a 1.2 min duration periodical flare emission at 4.86 GHz. A continuous tracking observation lasting 147 min is made by FAST at L-band in order not to miss the possible flare emission when slewing the telescope. The data reduction and calibration follow the same pipeline made for the FAST radio continuum [41]. Due to a lack of monitoring of the

reference position, the ArPLs algorithm is adopted for baseline fitting, which filters out the galactic background emission together with the possible quiescent emission component, and we have the chance to search for its flare emission. A careful search by eye and by wavelet analysis is made toward the flagged RFI and RFI-subtracted dynamic spectra in both total intensity I and circular polarization V . No significant radio flare emission can be solidly identified in our observation at the frequency range of 1.0–1.5 GHz, down to a sensitivity of about 13 mJy and 2 mJy (5σ level) in I and V , respectively. A few short-time blob structures are present in V . However, without high time resolution sampling, which may help reveal fine structures on sub-second time scale, it is difficult to distinguish them from RFI. Although the flare emission of 2MASSW J0746425 + 200032 is not successfully detected in our FAST L-band observation, we still emphasize the necessity of multiple frequencies, especially for low-frequency observations, regarding the fact that most of the currently existing observations have been made above 4 GHz. The radio flares occurring at different radio frequencies may originate from the different heights of stars. Therefore multi-frequency observations can help to delineate the magnetic field structures of stars and advance the understanding of the ECM at the lower-frequency end.

Statistics and analyses of the physical properties of radio stars was conducted by Zhang et al. [56]. Based on the research, we will select more radio stars (active stars, ultra-cool dwarfs, and host stars of exoplanets) for FAST observational objects. New target sources will be considered for upcoming observations to study the stellar radio emission of various radiation mechanisms, such as thermal bremsstrahlung, gyrosynchrotron, and plasma radiation [57].

Author Contributions: Conceptualization, L.Z.; Data curation, L.Z.; Investigation, X.L.H.; Project administration, L.Z.; Software, T.S., X.G. and Q.P.; Writing—original draft, T.S.; Writing—review & editing, L.Z., X.G., P.M. and X.L.H. All authors were informed about each step of manuscript processing including submission, revision, revision reminders, etc., via emails from our system or the assigned Assistant Editor. All authors have read and agreed to the published version of the manuscript.

Funding: We thank the anonymous referee for critical and enlightening comments. LYZ is supported by the Joint Fund of Astronomy of the NSFC and CAS Grant No. 11963002. XYG is supported by the National Natural Science Foundation of China (Grant Nos. 11833009, 11988101) and the CAS-NWO cooperation programme (Grant No. GJHZ1865). This research is also supported by the fostering project of GuiZhou University with No. 201911, the CSST project from the China Manned Space Project with No. CMS-CSST-2021-B07 and Cultivation Project for FAST Scientific Payoff and Research Achievement of CAMS-CAS.

Conflicts of Interest: The authors declare no conflict of interest.

References

1. Wendker, H.J. Radio continuum emission from stars: A catalogue update. *Astron. Astrophys. Suppl. Ser.* **1995**, *109*, 177–179.
2. Güdel, M. Stellar Radio Astronomy: Probing Stellar Atmospheres from Protostars to Giants. *Annu. Rev. Astron. Astrophys.* **2002**, *40*, 217–261.
3. Beasley, A.J.; Güdel, M. VLBA Imaging of Quiescent Radio Emission from UX Arietis. *Astrophys. J.* **2000**, *529*, 961–967. [[CrossRef](#)]
4. McGale, P.A.; Pye, J.P.; Hodgkin, S.T. ROSAT PSPC X-ray spectral survey of W UMa systems. *Mon. Not. R. Astron. Soc.* **1996**, *280*, 627–637. [[CrossRef](#)]
5. Gunn, A.G.; Brady, P.A.; Migenes, V.; Spencer, R.E.; Doyle, J.G. Eclipsing behaviour of the radio emission in the Algol system V505 Sagittarii. *Mon. Not. R. Astron. Soc.* **1999**, *304*, 611–621. [[CrossRef](#)]
6. Yu, S.; Doyle, J.G.; Kuznetsov, A.; Hallinan, G.; Antonova, A.; MacKinnon, A.L.; Golden, A. Electron-beam-induced Radio Emission from Ultracool Dwarfs. *Astrophys. J.* **2012**, *752*, 60.
7. Llama, J.; Jardine, M.M.; Wood, K.; Hallinan, G.; Morin, J. Simulating Radio Emission from Low-mass Stars. *Astrophys. J.* **2018**, *854*, 7.
8. Das, B.; Chandra, P.; Shultz, M.E.; Wade, G.A.; Sikora, J.; Kochukhov, O.; Neiner, C.; Oksala, M.E.; Alecian, E. Discovery of Eight “Main-sequence Radio Pulse Emitters” Using the GMRT: Clues to the Onset of Coherent Radio Emission in Hot Magnetic Stars. *Astrophys. J.* **2022**, *925*, 125.
9. Peterson, W.M.; Mutel, R.L.; Güdel, M.; Goss, W.M. A large coronal loop in the Algol system. *Nature* **2010**, *463*, 207–209. [[CrossRef](#)]

10. Aronow, R.A.; Herbst, W.; Hughes, A.M.; Wilner, D.J.; Winn, J.N. Optical and Radio Observations of the T Tauri Binary KH 15D (V582 Mon): Stellar Properties, Disk Mass Limit, and Discovery of a CO Outflow. *Astrophys. J.* **2018**, *155*, 47.
11. Helfand, D.J.; White, R.L.; Becker, R.H. The Last of FIRST: The Final Catalog and Source Identifications. *Astrophys. J.* **2015**, *801*, 26.
12. Kirkpatrick, J.D.; Reid, I.N.; Liebert, J.; Cutri, R.M.; Nelson, B.; Beichman, C.A.; Dahn, C.C.; Monet, D.G.; Gizis, J.E.; Skrutskie, M.F. Dwarfs Cooler than “M”: The Definition of Spectral Type “L” Using Discoveries from the 2 Micron All-Sky Survey (2MASS). *Astrophys. J.* **1999**, *519*, 802–833. [[CrossRef](#)]
13. Martín, E.L.; Delfosse, X.; Basri, G.; Goldman, B.; Forveille, T.; Zapatero Osorio, M.R. Spectroscopic Classification of Late-M and L Field Dwarfs. *Astrophys. J.* **1999**, *118*, 2466–2482. [[CrossRef](#)]
14. Kirkpatrick, J.D.; Gelino, C.R.; Cushing, M.C.; Mace, G.N.; Griffith, R.L.; Skrutskie, M.F.; Marsh, K.A.; Wright, E.L.; Eisenhardt, P.R.; McLean, I.S.; et al. Further Defining Spectral Type “Y” and Exploring the Low-mass End of the Field Brown Dwarf Mass Function. *Astrophys. J.* **2012**, *753*, 156.
15. Luhman, K.L. Discovery of a Binary Brown Dwarf at 2 pc from the Sun. *Astrophys. J. Lett.* **2013**, *767*, L1.
16. Luhman, K.L. Discovery of a ~250 K Brown Dwarf at 2 pc from the Sun. *Astrophys. J. Lett.* **2014**, *786*, L18.
17. Williams, P.K.G.; Cook, B.A.; Berger, E. Trends in Ultracool Dwarf Magnetism. I. X-ray Suppression and Radio Enhancement. *Astrophys. J.* **2014**, *785*, 9.
18. Güdel, M.; Benz, A.O. X-Ray/Microwave Relation of Different Types of Active Stars. *Astrophys. J. Lett.* **1993**, *405*, L63. [[CrossRef](#)]
19. Benz, A.O.; Güdel, M. X-ray/microwave ratio of flares and coronae. *Astron. Astrophys.* **1994**, *285*, 621–630.
20. Tang, J.; Tsai, C.W.; Li, D. The Potential of Detecting Radio-flaring Ultracool Dwarfs at L band in the FAST Drift-scan Survey. *Res. Astron. Astrophys.* **2022**, *22*, 65013.
21. Berger, E.; Rutledge, R.E.; Reid, I.N.; Bildsten, L.; Gizis, J.E.; Liebert, J.; Martín, E.; Basri, G.; Jayawardhana, R.; Brandeker, A.; et al. The Magnetic Properties of an L Dwarf Derived from Simultaneous Radio, X-ray, and H α Observations. *Astrophys. J.* **2005**, *627*, 960–973.
22. Hallinan, G.; Antonova, A.; Doyle, J.G.; Bourke, S.; Lane, C.; Golden, A. Confirmation of the Electron Cyclotron Maser Instability as the Dominant Source of Radio Emission from Very Low Mass Stars and Brown Dwarfs. *Astrophys. J.* **2008**, *684*, 644–653.
23. Reid, I.N.; Gizis, J.E.; Kirkpatrick, J.D.; Koerner, D.W. A Search for L Dwarf Binary Systems. *Astrophys. J.* **2001**, *121*, 489–502.
24. Dahn, C.C.; Harris, H.C.; Vrba, F.J.; Guetter, H.H.; Canzian, B.; Henden, A.A.; Levine, S.E.; Luginbuhl, C.B.; Monet, A.K.B.; Monet, D.G.; et al. Astrometry and Photometry for Cool Dwarfs and Brown Dwarfs. *Astrophys. J.* **2002**, *124*, 1170–1189.
25. Bouy, H.; Duchêne, G.; Köhler, R.; Brandner, W.; Bouvier, J.; Martín, E.L.; Ghez, A.; Delfosse, X.; Forveille, T.; Allard, F.; et al. First determination of the dynamical mass of a binary L dwarf. *Astron. Astrophys.* **2004**, *423*, 341–352. :20040551. [[CrossRef](#)]
26. Reid, I.N.; Kirkpatrick, J.D.; Gizis, J.E.; Dahn, C.C.; Monet, D.G.; Williams, R.J.; Liebert, J.; Burgasser, A.J. Four Nearby L Dwarfs. *Astrophys. J.* **2000**, *119*, 369–377.
27. Berger, E.; Rutledge, R.E.; Phan-Bao, N.; Basri, G.; Giampapa, M.S.; Gizis, J.E.; Liebert, J.; Martín, E.; Fleming, T.A. Periodic Radio and H α Emission from the L Dwarf Binary 2MASSW J0746425 + 200032: Exploring the Magnetic Field Topology and Radius of an L Dwarf. *Astrophys. J.* **2009**, *695*, 310–316.
28. Harding, L.K.; Hallinan, G.; Konopacky, Q.M.; Kratter, K.M.; Boyle, R.P.; Butler, R.F.; Golden, A. Spin-orbit alignment in the very low mass binary regime. The L dwarf tight binary 2MASSW J0746425 + 200032AB. *Astron. Astrophys.* **2013**, *554*, A113.
29. Zhang, Q.; Hallinan, G.; Briske, W.; Bourke, S.; Golden, A. Multiepoch VLBI of L Dwarf Binary 2MASS J0746 + 2000AB: Precise Mass Measurements and Confirmation of Radio Emission from Both Components. *Astrophys. J.* **2020**, *897*, 11.
30. Zic, A.; Lynch, C.; Murphy, T.; Kaplan, D.L.; Chandra, P. Low-frequency GMRT observations of ultra-cool dwarfs. *Mon. Not. R. Astron. Soc.* **2019**, *483*, 614–623.
31. Nan, R.; Li, D.; Jin, C.; Wang, Q.; Zhu, L.; Zhu, W.; Zhang, H.; Yue, Y.; Qian, L. The Five-Hundred Aperture Spherical Radio Telescope (fast) Project. *Int. J. Mod. Phys. D* **2011**, *20*, 989–1024.
32. Condon, J.J. Confusion and Flux-Density Error Distributions. *Astrophys. J.* **1974**, *188*, 279–286. [[CrossRef](#)]
33. Condon, J.J. Extragalactic Astronomy at Low Frequencies. In Proceedings of the from Clark Lake to the Long Wavelength Array: Bill Erickson’s Radio Science, Santa Fe, NM, USA, 8–11 September 2004; Kassim, N., Perez, M., Junor, W., Henning, P., Eds.; Astronomical Society of the Pacific Conference Series; NASA: Washington, DC, USA, 2005; Volume 345, p. 237.
34. Hallinan, G.; Bourke, S.; Lane, C.; Antonova, A.; Zavala, R.T.; Briske, W.F.; Boyle, R.P.; Vrba, F.J.; Doyle, J.G.; Golden, A. Periodic Bursts of Coherent Radio Emission from an Ultracool Dwarf. *Astrophys. J. Lett.* **2007**, *663*, L25–L28.
35. Antonova, A.; Doyle, J.G.; Hallinan, G.; Bourke, S.; Golden, A. A mini-survey of ultracool dwarfs at 4.9 GHz. *Astron. Astrophys.* **2008**, *487*, 317–322. [[CrossRef](#)]
36. Route, M.; Wolszczan, A. The Arecibo Detection of the Coolest Radio-flaring Brown Dwarf. *Astrophys. J. Lett.* **2012**, *747*, L22.
37. Williams, P.K.G.; Berger, E.; Irwin, J.; Berta-Thompson, Z.K.; Charbonneau, D. Simultaneous Multiwavelength Observations of Magnetic Activity in Ultracool Dwarfs. IV. The Active, Young Binary NLTT 33370 AB (=2MASS J13142039 + 1320011). *Astrophys. J.* **2015**, *799*, 192.
38. Williams, P.K.G.; Berger, E. The Rotation Period and Magnetic Field of the T Dwarf 2MASSI J1047539+212423 Measured from Periodic Radio Bursts. *Astrophys. J.* **2015**, *808*, 189.
39. Zarka, P.; Li, D.; Griesmeier, J.M.; Lamy, L.; Girard, J.N.; Hess, S.L.G.; Lazio, T.J.W.; Hallinan, G. Detecting exoplanets with FAST? *Res. Astron. Astrophys.* **2019**, *19*, 23.
40. Treumann, R.A. The electron-cyclotron maser for astrophysical application. *Astron. Astrophys. Rev.* **2006**, *13*, 229–315. [[CrossRef](#)]

41. Gao, X.; Reich, W.; Sun, X.; Zhao, H.; Hong, T.; Yuan, Z.; Reich, P.; Han, J. Peering into the Milky Way by FAST: IV. Identification of two new Galactic supernova remnants G203.1 + 6.6 and G206.7 + 5.9. *Sci. China Physics, Mech. Astron.* **2022**, *65*, 129705.
42. Sun, X.H.; Meng, M.N.; Gao, X.Y.; Reich, W.; Jiang, P.; Li, D.; Yan, H.R.; Li, X.H. New continuum and polarization observations of the Cygnus Loop with FAST I. Data processing and verification. *Res. Astron. Astrophys.* **2021**, *21*, 282. [[CrossRef](#)]
43. Jiang, P.; Tang, N.Y.; Hou, L.G.; Liu, M.T.; Krčo, M.; Qian, L.; Sun, J.H.; Ching, T.C.; Liu, B.; Duan, Y.; et al. The fundamental performance of FAST with 19-beam receiver at L band. *Res. Astron. Astrophys.* **2020**, *20*, 64.
44. Ching, T.C.; Li, D.; Heiles, C.; Li, Z.Y.; Qian, L.; Yue, Y.L.; Tang, J.; Jiao, S.H. An early transition to magnetic supercriticality in star formation. *Nature* **2022**, *601*, 49–52.
45. Baek, S.J.; Park, A.; Ahn, Y.J.; Choo, J. Baseline correction using asymmetrically reweighted penalized least squares smoothing. *Analyst* **2015**, *140*, 250–257. [[CrossRef](#)]
46. Zhang, J.; Tian, H.; Zarka, P.; Louis, C.K.; Lu, H.; Gao, D.; Sun, X.; Yu, S.; Chen, B.; Cheng, X.; et al. Fine structures of radio bursts from flare star AD Leo with FAST observations. *arXiv* **2023**, arXiv:2306.00895. [[CrossRef](#)]
47. Cenacchi, E.; Kraus, A.; Orfei, A.; Mack, K.H. Full Stokes polarimetric observations with a single-dish radio telescope. *Astron. Astrophys.* **2009**, *498*, 591–599.
48. Myserlis, I.; Angelakis, E.; Kraus, A.; Lontas, C.A.; Marchili, N.; Aller, M.F.; Aller, H.D.; Karamanavis, V.; Fuhrmann, L.; Krichbaum, T.P.; et al. Full-Stokes polarimetry with circularly polarized feeds. Sources with stable linear and circular polarization in the GHz regime. *Astron. Astrophys.* **2018**, *609*, A68.
49. Wang, Y.; Zhang, H.Y.; Hu, H.; Huang, S.J.; Zhu, W.W.; Zhi, G.P.; Zhang, T.; Fan, Z.C.; Yang, L. Satellite RFI mitigation on FAST. *Res. Astron. Astrophys.* **2021**, *21*, 18. [[CrossRef](#)]
50. Zhang, C.P.; Xu, J.L.; Wang, J.; Jing, Y.; Liu, Z.; Zhu, M.; Jiang, P. Radio Frequency Interference Mitigation and Statistics in the Spectral Observations of FAST. *Res. Astron. Astrophys.* **2022**, *22*, 25015.
51. Yao, J.M.; Manchester, R.N.; Wang, N. A New Electron-density Model for Estimation of Pulsar and FRB Distances. *Astrophys. J.* **2017**, *835*, 29.
52. Berger, E.; Basri, G.; Fleming, T.A.; Giampapa, M.S.; Gizis, J.E.; Liebert, J.; Martín, E.; Phan-Bao, N.; Rutledge, R.E. Simultaneous Multi-Wavelength Observations of Magnetic Activity in Ultracool Dwarfs. III. X-ray, Radio, and H α Activity Trends in M and L dwarfs. *Astrophys. J.* **2010**, *709*, 332–341.
53. Melrose, D.B.; Dulk, G.A. Electron-cyclotron masers as the source of certain solar and stellar radio bursts. *Astrophys. J.* **1982**, *259*, 844–858. [[CrossRef](#)]
54. Robinson, P.A. Escape of Fundamental Electron-Cyclotron Maser Emission from the Sun and Stars. *Astrophys. J. Lett.* **1989**, *341*, L99. [[CrossRef](#)]
55. Osten, R.A.; Hawley, S.L.; Bastian, T.S.; Reid, I.N. The Radio Spectrum of TVLM 513-46546: Constraints on the Coronal Properties of a Late M Dwarf. *Astrophys. J.* **2006**, *637*, 518–521.
56. Zhang, L.; Cheng, Y.; Han, X.L.; Pi, Q.; Misra, P.; Li, B.; Zhu, Z. Physical Properties of Radio Stars Based on LAMOST Spectral Survey. *Universe* **2022**, *8*, 384. [[CrossRef](#)]
57. Matthews, L.D. Radio Stars: From kHz to THz. *Publ. Astron. Soc. Pac.* **2019**, *131*, 16001.

Disclaimer/Publisher’s Note: The statements, opinions and data contained in all publications are solely those of the individual author(s) and contributor(s) and not of MDPI and/or the editor(s). MDPI and/or the editor(s) disclaim responsibility for any injury to people or property resulting from any ideas, methods, instructions or products referred to in the content.